Efficient frequency conversion in slab waveguide by cascaded nonreciprocal interband photonic transitions

Hwi Kim[1,*] and Byoungho Lee[2]

[1]*Department of Electronics and Information Engineering, College of Science and Technology, Sejong Campus, Korea University, Jochiwon-eup, Yeongi-gun, Chungnam, 339-700, Korea*

[2]*National Creative Research Center for Active Plasmonics Application Systems, Inter-University Semiconductor Research Center and School of Electrical Engineering, Seoul National University, Gwanak-Gu Gwanakro 599, Seoul, 151-744, Korea*

**Corresponding author: hwikim@korea.ac.kr*

Received June 28, 2010; revised August 28, 2010; accepted August 28, 2010; posted August 31, 2010 (Doc. ID 130761); published September 20, 2010

A slab-waveguide-based configuration for efficient frequency conversion is proposed. In the proposed structure, frequency conversion is induced through cascaded multistep nonreciprocal interband photonic transitions activated by external refractive-index modulations. The advantages of interband photonic transition over intraband photonic transition for frequency conversion are analyzed with the coupled-mode theory.

OCIS codes: 160.5293, 130.7405.

Investigation on the analogy of photonics to electronics creates great opportunity to invent novel concepts and technological breakthroughs that can overcome the fundamental limitations of modern electronics in bandwidth, speed, and capacity. In this context, we see a strong need for investigating the inter- or intraband transition mechanism of photons in photonic structures for reaching the full potential of photonic devices.

Recently, Yu and Fan proposed a novel mechanism of complete optical isolation by nonreciprocal interband photonic transitions using time-varying structural refractive-index perturbation [1,2]. The nonreciprocal interaction of light and matter has been researched intensively owing to its fundamental importance [3–5], which provides a basic mechanism for realizing novel photonic devices, such as a photonic isolator, diode, and transistor. It was also shown that frequency conversion is enabled in a nonreciprocal linear manner using time-varying structural refractive-index perturbation. Frequency conversion can be realized by several mechanisms as nonlinear harmonic generation [5], Doppler shift in dynamically tuned microcavities [6], and so on. Interestingly, frequency conversion and linear and nonlinear nonreciprocal interactions are closely related and occur simultaneously in many cases.

In this Letter, we propose a configuration of cascaded multistep linear nonreciprocal interband transitions for efficient frequency conversion in a slab waveguide with time-varying structural refractive-index perturbation. In the proposed structure, frequency conversion is induced through interband or intraband photonic transition, and the amount of frequency change can be controlled arbitrarily. This is a distinctive point from frequency conversion by nonlinear harmonic generation. Considering that the dynamic range of single-step frequency conversion with a single photonic band transition is limited to be small, we address the multistep photonic band transition as an effective manner to attain large frequency variation.

The frequency conversion processes in a slab waveguide are divided into two ways principally: intraband photonic transition and interband photonic transition. The frequency conversion based on interband and intraband transitions can be analyzed with the coupled-mode theory. Consider a slab waveguide with a width of w and a permittivity of ε_S. As in [1], this slab waveguide is supposed to have a localized single modulation region, where the perturbation of permittivity is given by $\varepsilon'(r,t) = \delta(x)\cos(qz - \Omega t)$, as shown in Fig. 1(a), which occupies one half of the slab waveguide. In practice, this kind of modulation would be realized by electrical and optical impact ionization structures [6,7], optomechanical crystals [8], and so on. In the coupled-mode theory of a single transition of $(\omega_i, \beta_i) \rightarrow (\omega_f, \beta_f)$ induced by the permittivity perturbation $\varepsilon'(r,t)$, three related optical modes are included. The y-directional electric field in the structure is represented by the coupled-mode analysis form

$$E(r,t) = a_i(z)E_i(x)e^{j(\beta_i z - \omega_i t)} + a_f(z)E_f(x)e^{j(\beta_f z - \omega_f t)} + a_n(z)E_n(x)e^{j(\beta_n z - \omega_n t)}, \quad (1)$$

where $E_i(x)e^{j(\beta_i z - \omega_i t)}$, $E_f(x)e^{j(\beta_f z - \omega_f t)}$, and $E_n(x)e^{j(\beta_n z - \omega_n t)}$ are normalized eigenmodes having unit power equal to 1. $a_i(z)$, $a_f(z)$, and $a_n(z)$ indicate the optical power flux of the respective modes. The first mode is the initial mode, E_i with ω_i and β_i, and the second mode is the transition mode, E_f with $\omega_f = \omega_i + \Omega$ and wavenumber β_f. The phase mismatch in this transition is denoted by $\Delta\beta_{i,f} = \beta_f - \beta_i - q$. The third mode is denoted by E_n with a frequency of $\omega_n = \omega_i - \Omega$ and wavenumber β_n. The phase mismatch in this interband transition is denoted by $\Delta\beta_{i,n} = \beta_n - \beta_i + q$. The wavenumbers are determined by the dispersion relation of the slab waveguide.

By substituting Eq. (1) into Maxwell's equations, we obtain the following coupled-mode equation system under the slowly varying amplitude approximation as

$$\begin{pmatrix} da_i(z)/dz \\ da_f(z)/dz \\ da_n(z)/dz \end{pmatrix} = \begin{pmatrix} 0 & jC_{i,f}e^{j\Delta\beta_{i,f}z} & jC_{i,n}e^{j\Delta\beta_{i,n}z} \\ jC_{f,i}e^{-j\Delta\beta_{i,f}z} & 0 & \\ jC_{n,i}e^{-j\Delta\beta_{i,n}z} & & 0 \end{pmatrix} \times \begin{pmatrix} a_i(z) \\ a_f(z) \\ a_n(z) \end{pmatrix}, \tag{2}$$

where the coupling parameters, $C_{i,f}$, $C_{f,i}$, $C_{i,n}$, and $C_{n,i}$, are given, respectively, by $C_{a,b} = (\varepsilon_0\omega_a/8)\int_{-\infty}^{\infty}\delta(x) \times E_a(x)E_b(x)\mathrm{d}x$, for $(a,b) = (i,f), (f,i), (i,n)$, and (n,i). Equation (2) can be numerically solved by the fourth-order Runge–Kutta method.

Figure 1(a) shows the simulation result of the interband transition between symmetric mode p_1 and asymmetric mode p_2. In the simulations, the slab waveguide thickness of $w = 0.22\ \mu$m, the permittivity of $\varepsilon_S = 12.25$, the first-mode frequency of $\omega_1 = 0.9$, and the second-mode frequency of $\omega_2 = 1.15$ are used. The value of frequency is a normalized value by $2\pi c/a$, where c and a are light speed in vacuum and 1 μm, respectively. The length of modulation region is set to 21.9 μm. The coupled-mode theory shows that the optical power is exchanging between symmetric mode p_1 and asymmetric mode p_2 along the z axis. The modulation invokes the variation of the total optical power conveyed by the optical modes as well as mode conversion. The high-frequency mode has higher power because the photon energy is proportional to frequency. It can be understood that the energy of the carrier signal is added to or subtracted from optical mode propagating in the slab waveguide. In Fig. 1(b), the electric field profile showing the interband photonic transitions is presented. In the band diagram, this kind of transition can be graphically

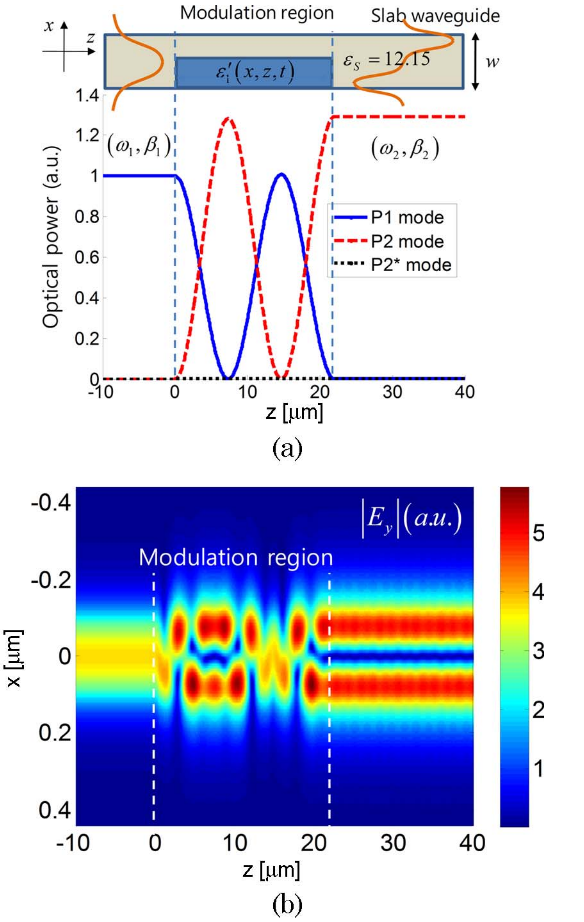

Fig. 1. (Color online) (a) Interband photonic transition in a slab waveguide between symmetric mode $p_1(\omega_1,\beta_1)$ and asymmetric mode $p_2(\omega_2,\beta_2)$. (b) y-directional electric field distribution $|E_y|$.

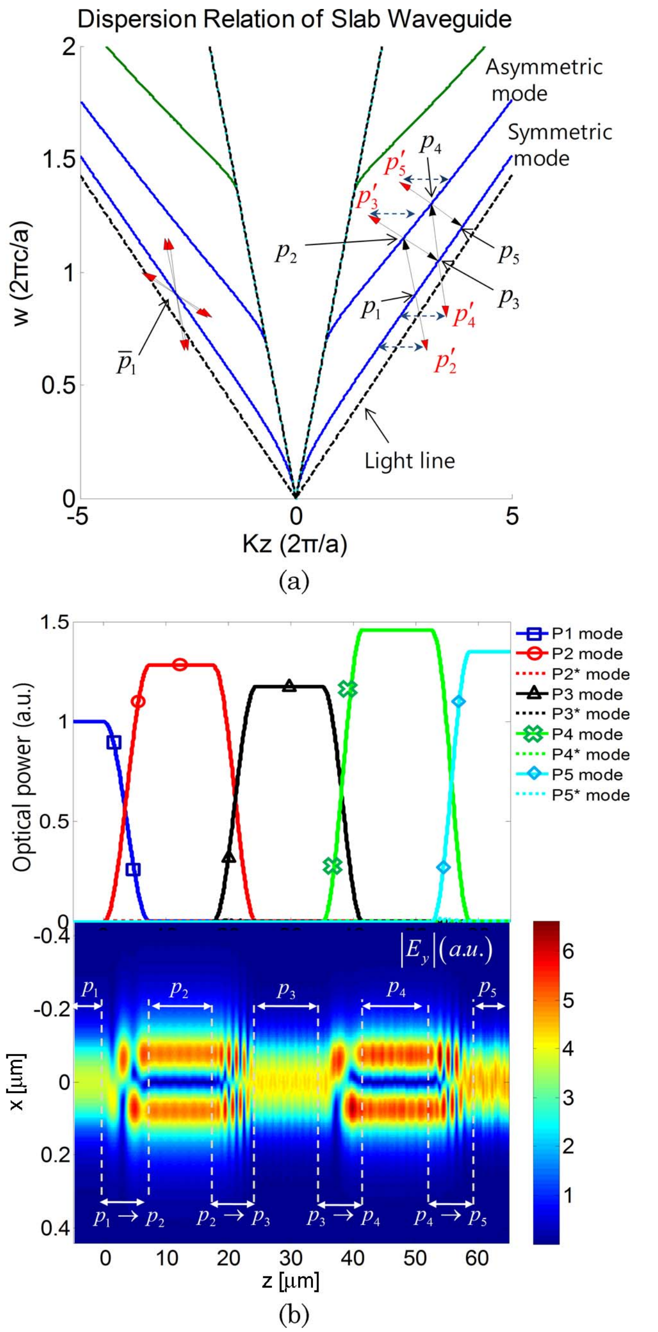

Fig. 2. (Color online) Cascaded multistep interband photonic transitions: (a) four-step interband photonic transitions ($p_1 \to p_2 \to p_3 \to p_4 \to p_5$); (b) optical power exchange along the z axis and y-directional electric field distribution $|E_y|$.

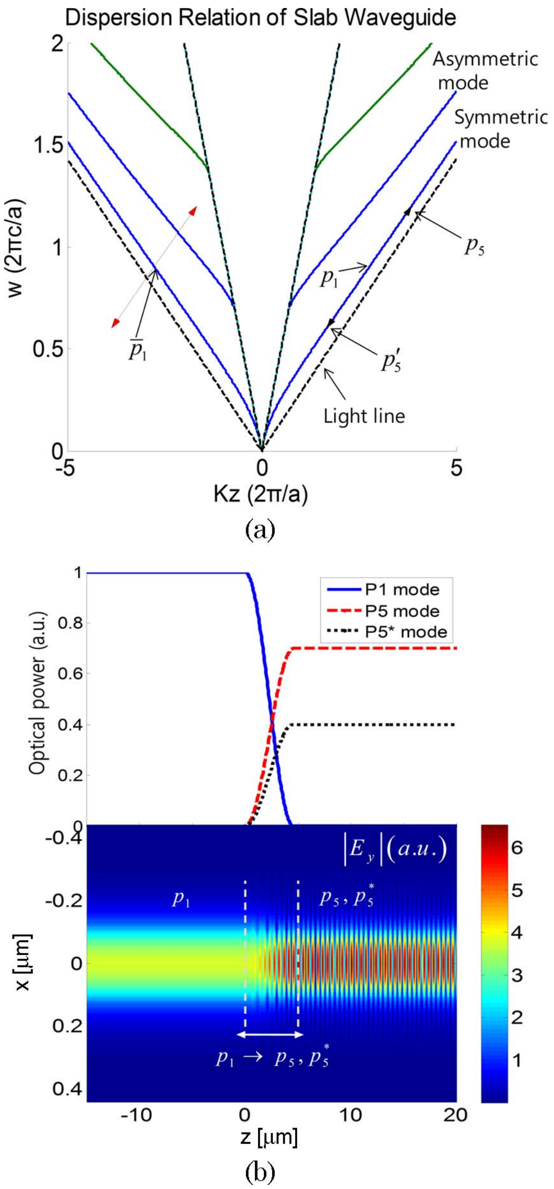

Fig. 3. (Color online) Single-steps intraband photonic transitions: (a) single-step intraband photonic transition ($p_1 \to p_5$ and $p_1 \to p_5'$); (b) optical power exchange along the z axis and y-directional electric field distribution $|E_y|$.

represented. Figure 2 shows the photonic band diagram with the information of mode transitions. The transition shown in Fig. 1 is denoted by the arrow from $p_1(\omega_1, \beta_1)$ to $p_2(\omega_2, \beta_2)$ in Fig. 2(a). In Fig. 2(a), the cascaded interband phtonic transitions—symmetric mode $p_1(\omega_1 = 0.9) \to$ asymmetric mode $p_2(\omega_2 = 1.15) \to$ symmetric mode $p_3(\omega_3 = 1.05) \to$ asymmetric mode $p_4(\omega_4 = 1.3) \to$ symmetric mode, $p_5(\omega_5 = 1.2)$—are graphically expressed. The nonexcitable modes due to large phase mismatch (denoted by horizontal dashed lines), which are included in Eq. (1), are denoted by p_2', p_3', p_4', and p_5'. Cascading multiple interband photonic transitions enable mode frequency to increase or decrease stepwise. In Fig. 2(b), the electric field profile of the four-step interband transitions with the indication of modulation regions is shown, and the optical power exchange along the z axis of each mode is plotted. It is seen that the optical power is dependent on optical frequency. The input optical mode with optical frequency of ω_1 is efficiently converted to the final optical mode with optical frequency of ω_5 through the multistep of interband transitions represented in Figs. 2(a) and 2(b). The optimal lengths of the modulation regions providing maximum frequency conversion efficiency are obtained as $l_{p_1\to p_2} = 7.3\ \mu$m, $l_{p_2\to p_3} = 6.85\ \mu$m, $l_{p_3\to p_4} = 6.4\ \mu$m, and $l_{p_4\to p_5} = 6.05\ \mu$m from the numerical calculation data.

In the case of a single intraband transition, two transitions to higher frequency mode, $p_1 \to p_5$, and lower frequency mode, $p_1 \to p_5'$, occur simultaneously, as shown in Fig. 3(a), which is the origin of inefficiency in frequency conversion. In Fig. 3(b), the length of the optimal modulation region is $l_{p_1\to p_5} = 4.55\ \mu$m. As shown in Fig. 3(b), the optical beating induced by two coherently superposed optical modes p_5 and p_5' is observed after the modulation region and the optical power exchange along the z axis is presented.

Comparing interband and intraband photonic transitions, we can see that the frequency conversion efficiency of the proposed multistep interband transitions is above 90%, which is two-times superior to that of the single intraband transitions less than 50%. Cascaded n-step intraband transitions would give low conversion efficiency less than $(50\%)^n$. The proposed multistep configuration with large dynamic range of frequency conversion can provide the physical mechanism necessary for advanced photonic devices, such as photonic diodes, modulators, and transistors.

The authors acknowledge the support by the National Research Foundation and the Ministry of Education, Science and Technology of Korea through the Creative Research Initiative Program (Active Plasmonics Applications Systems).

References

1. Z. Yu and S. Fan, Nat. Photon. **3**, 91 (2009).
2. Z. Yu and S. Fan, Appl. Phys. Lett. **94**, 171116 (2009).
3. C. E. Rüter, K. G. Makris, R. El-Ganainy, D. N. Christodoulides, M. Segev, and D. Kip, Nature Phys. **6**, 192 (2010).
4. X. Zang and C. Jiang, J. Opt. Soc. Am. B **26**, 2275 (2009).
5. V. V. Konotop and V. Kuzmiak, Phys. Rev. B **66**, 235208 (2002).
6. S. F. Preble, Q. Xu, and M. Lipson, Nat. Photon. **1**, 293 (2007).
7. Q. Xu, B. Schmidt, S. Pradhan, and M. Lipson, Nature **435**, 325 (2005).
8. M. Eichenfield, J. Chan, R. M. Camacho, K. J. Vahala, and O. Painter, Nature **462**, 78 (2009).